

Morphological and chemical characterization of oxide films produced by plasma anodization of 5052 aluminum alloy in solution containing sodium silicate and sodium phosphate

Caracterização morfológica e química de filmes óxidos produzidos por anodização a plasma da liga de alumínio 5052 em solução contendo silicato de sódio e fosfato de sódio

Rafael Resende Lucas¹, Leide Lili Gonçalves Silva¹, Deborah Cristina Ribeiro dos Santos¹

ABSTRACT

Plasma anodization or plasma electrolytic process is a treatment that has been studied for surface modification of various alloys, mainly light alloys such as Al, Mg and Ti. The different combinations among the process parameters allow the deposition of oxide films with diverse or functional properties, which obviously depend on the morphological and chemical characteristics of the film structures. This work shows the results of plasma anodization used in the treatment of 5052 aluminum alloy, using a basic electrolyte solution containing sodium silicate (Na_2SiO_3) and small proportions of sodium phosphate (Na_3PO_4). X-ray diffraction (XRD) and infrared (IR) spectroscopy were used for chemical structural analysis of the films, and the surface morphology of the samples was investigated by a scanning electron microscope (SEM). The films resulting from the processes are basically alumina (Al_2O_3) combined with silicate, with a slightly rough and porous surface, and thickness in the order of micrometers. Corrosion tests carried out in NaCl solution (3.5 wt%) show that all films have a higher chemical resistance compared to the bare 5052 Al alloy.

Keywords: Anodization, XRD, Corrosion.

RESUMO

A anodização a plasma ou processo eletrolítico a plasma é um tratamento que tem sido estudado para modificação superficial de várias ligas, principalmente ligas leves tais como Al, Mg e Ti. As diferentes combinações entre os parâmetros do processo permitem a deposição de filmes óxidos com propriedades diversificadas ou funcionais, que obviamente dependem das características morfológicas e químicas das estruturas dos filmes. Este trabalho mostra os resultados da anodização a plasma usada no tratamento da liga de alumínio 5052, usando uma solução eletrolítica básica contendo silicato de sódio (Na_2SiO_3) e pequenas proporções de fosfato de sódio (Na_3PO_4). A difração de raios-X (DRX) e a espectroscopia por infravermelho (IV) foram empregadas para análise estrutural química dos filmes, e a morfologia superficial das amostras foi investigada por um microscópio eletrônico de varredura (MEV). Os filmes resultantes dos processos são basicamente de alumina (Al_2O_3) combinada com silicato, com superfície levemente rugosa e porosa, e espessura na ordem de micrometros. Ensaio de corrosão realizados em solução de NaCl (3.5 wt%) mostram que todos os filmes apresentam maior resistência química comparada com a liga Al 5052 sem tratamento.

Palavras-chave: Anodização, DRX, Corrosão.

¹Centro Estadual de Educação Tecnológica "Paula Souza" – Faculdade de Tecnologia de Pindamonhangaba – Pindamonhangaba (SP), Brasil.

*Corresponding author: rresendelucas@gmail.com

Received: 3 Feb 2020 Accepted: 30 Mar 2020

INTRODUCTION

Anodizing is an industrial process widely employed in surface modification of aluminum and its alloys, aimed at improving the wear and corrosion resistance and, consequently, prolonging their lifespan. Conventional anodizing is usually performed on acid electrolytes that demand care with gases exhaustion and waste disposal. whereas hard anodizing employs hexavalent chrome, which is carcinogenic¹. Therefore, clean technologies are important to environment and workers, and plasma processes are alternative techniques for surface treatments. Atmospheric-pressure plasma is economically viable compared to low-pressure plasma (vacuum technology), and it can be established in electrolytic solution employing high voltage (hundreds to thousands of volts)².

The combination between plasma and anodizing processes appends chemical, thermal and electrical reactions on metal/alloy surface, producing oxide films with different crystalline and morphological structures². Besides, dependent on the process parameters (voltage, current density, temperature, process time, electrolyte composition, metal/alloy composition, among others related to electrolytic system), the mechanical and tribological properties of oxide films can be better than those films obtained from conventional anodizing³. Furthermore, the physical and chemical mechanisms associated to plasma electrolysis allow anodization to be accomplished in a single step, in a short period (few minutes or seconds), in alkaline or basic aqueous solutions, even on nonconventional anodized alloys, ensuring high adhesion to substrate¹.

Particularly, the electrolytic plasma process is highly attractive for the treatment of light alloys due to the average process temperature, which is lower than the boiling point of water². In literature, there are studies about the plasma electrolytic process applied for modification of different alloys, such as Al, Mg, Ti, Zr, Ni e Ta⁴⁻⁸. Those works present the process with other denominations, such as plasma electrolytic oxidation (PEO), microarc oxidation (MAO), microplasma oxidation (MPO), plasma electrolytic anodic treatment, spark anodic oxidation, spark anodizing, and others⁹. However, oxidation by electrolysis occurs in the anodic electrode and, for this reason, it is called plasma anodization (PA) in this work.

Considering the novel character of the technology and many possibilities of parameter combinations (electric, chemical and thermic), this work shows the effect of electrolyte composition on the morphology of the films grown on 5052 aluminum alloy deposited by PA. The 5052 aluminum alloy presents a high content of magnesium (2–3%) and, hence, high corrosion resistance, being typically applied in marine and aircraft industries¹. There are few papers in literature showing the effect of PA on this alloy; so, this work evaluates the effect of a basic electrolytic solution composed by sodium silicate (Na_2SiO_3) and small proportions of sodium phosphate (Na_3PO_4).

Silicate favors the growth rate of the oxide layers³ and it is expected that phosphate improve their corrosion resistance¹⁰. Due to the competition between PO_4^{3-} and SiO_3^{2-} in the electrolyte during the formation of the coatings¹¹, phosphate was limited to less than 15% of silicate. Chemical and morphological analysis of PA-treated samples were accomplished by infrared spectroscopy (FTIR), X-ray diffraction (XRD) and scanning electronic microscopy (SEM). Dispersive energy detector (EDX) coupled to the SEM was used for elemental chemical evaluation of oxide films. Finally, electrochemical analysis conducted via potentiodynamic polarization tests was applied to determine the corrosion resistance of PA-treated samples.

METHODS

Small substrates ($20 \times 20 \times 2$ mm) of commercial 5052 aluminum alloy were ground with abrasive papers (600–1200#), washed in neutral detergent and tap water, and rinsed with distilled water. Following, they were immersed in isopropyl alcohol, submitted to ultrasonic cleaning for 15 min, and dried with a hot air blower. Chemical composition of 5052 Al alloy was informed as: 95.75–96.55% Al, 2.20–2.80% Mg, 0.40% Fe, 0.15–0.35% Cr, 0.25% Si, 0.10% Zn, 0.10% Cu, 0.10% Mn, 0.15% others. Electrolytic solution (pH 13) was prepared with distilled water, 15 g/L of sodium silicate (Na_2SiO_3) and sodium phosphate (Na_3PO_4) in the following proportions: 1.0, 1.5 and 2.0 g/L. Both chemical products with 98% of purity were purchased from Dinâmica Química Contemporânea Ltd. The electrolytic plasma system comprises a 20 kW high-voltage DC power supply (CTRLTECH CCY 1000–20DA1A), a mechanical stirrer (FISATOM 710), two multimeters (MINIPA ET2030A), a thermometer (MINIPA ET401A), and a Pyrex glass beaker (2000 ml) as the electrolytic cell, as shown in Fig. 1. In this system, a counter-electrode (24×10 cm) adjusted in the round beaker was prepared from a 3 mm-sheet of 1200 Al alloy. The PA processes were sustained by a 420 V-voltage for 10 min, reaching a temperature of 40 °C.

The surface morphology and chemical composition of PA-treated films were evaluated by a JEOL JSM-6010LA system, composed by a scanning electron microscope (SEM) with energy-dispersive X-ray spectroscopy (EDX). Crystallinity composition of those films was analyzed by X-ray diffraction (XRD) using a PANalytical X'PERT PRO equipment with Cu K α radiation ($\lambda = 0.154$ nm, 40 KV and 40 mA), scanning 2θ from 15°–90° with a 0.05° step size. Molecular structure of oxide films was also evaluated by infrared spectroscopy (IR) using a JASCO FT/IR 410 system, scanning wavenumber range 4000–400 cm^{-1} , and the spectra were obtained from 124 scans with resolution of 4 cm^{-1} . Roughness of the samples was measured by a VEECO Dektak-150 profilometer, using a 12.5 μm -radius indenter, 2000.0 μm -length scan, 3.00 mg-force and 15 s of duration. An Eddy-current gauge was used to measure the thickness of the films.

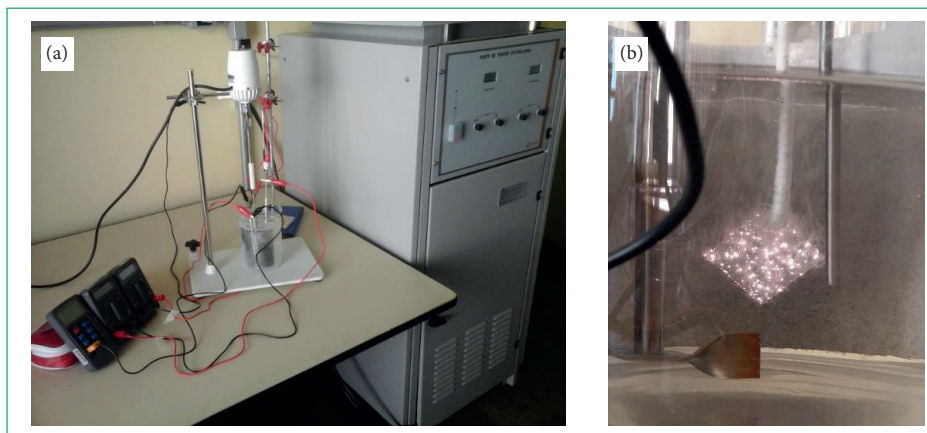


Figure 1: Images of DC electrolytic system (a) and PA process on Al sample (b).

Electrochemical analysis for determination of corrosion resistance was performed according to the standard reference test method for making potentiodynamic anodic polarization measurements (ASTM G5-14).

A Metrohm Autolab PGstat302N Galvanostat/Potentiostat, operated by software General Purpose Electrochemical System (GPES), was employed for this analysis, and a conventional 250 ml-glass cell fitted with three electrodes, specifically: the substrate as working-electrode, Pt wire as counter-electrode, and Ag/AgCl (KCl_{sat}) as reference-electrode. The surface area of the examined samples exposed to corrosive medium was about 0.8 cm^2 . Corrosive solution was prepared with NaCl (99 % of purity), which was purchased from Merck. Prior to corrosion tests, working-electrode was immersed in 3.5 wt% NaCl solution for 86400 s in a controlled temperature of $23 \text{ }^\circ\text{C}$ to stabilize the corrosion potential (E_{corr}). Then, Tafel polarization curves were obtained over a potential range from -1.2 to $+0.2 \text{ V}$ using scan rate of 0.33 mV/s . Corrosion current densities (I_{corr}) were determined by linear extrapolation of the polarization curves up to $\pm 50 \text{ mV}$ from E_{corr} .

RESULTS AND DISCUSSION

FTIR analysis

Figure 2 depicts the infrared spectra of the untreated 5052 aluminum alloy and oxide films produced via plasma anodization with different Na_3PO_4 proportions in silicate-containing solutions.

Aluminum alloy spectrum in Fig. 2 presents a short band at $1000\text{--}400 \text{ cm}^{-1}$ assigned to nanometric alumina (Al_2O_3) grown under atmosphere oxidation¹², and a short band at $2700\text{--}1300 \text{ cm}^{-1}$ probably related to other species adsorbed on the alumina from environment, such as CO_2 and/or H_2O ¹³. However, observing the PEO film spectra, the same vibration bands can be noticed: a broad band at $3650\text{--}2700\text{-cm}^{-1}$ assigned to OH stretching, related to free H_2O ¹³ and hydroxides, such as NaOH or AlOH_3 ¹²; the shoulder at 3650-cm^{-1} and the peak centered at 1640 cm^{-1} are attributed, respectively, to OH stretching and OH bending, confirming H_2O adsorbed on film

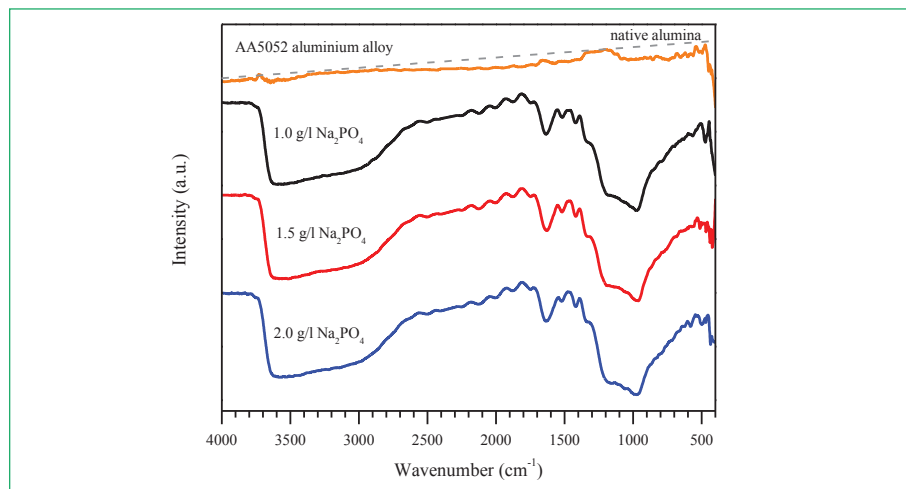


Figure 2: FTIR spectra of untreated and PA-treated aluminum alloy.

surface¹⁴; a small peak at 1555 cm⁻¹ assigned to Al–OH bonds¹² and/or CO stretching in CO₂ adsorbed on the surface¹⁵; a broad band around 1200–970 cm⁻¹ assigned to Si–O–Si and Si–O–Al groups, because Al and Si present similar masses which leads to same vibration frequencies¹⁶. Below 1000 cm⁻¹, there are absorptions from alumina (Al₂O₃) at different atom coordination^{12,14,17,18}, as well as vibrations from silica (Si–O₂) and mullite (3Al₂O₃·SiO₂)¹⁹.

Stretching and/or bending in AlO₄ groups is identified by the shoulder at 970 cm⁻¹, which is directly related to γ -Al₂O₃ crystalline phase¹⁷. Small peaks observed from 550 to 400 cm⁻¹ can be attributed to bedding in condensed AlO₄ and stretching in isolated AlO₆¹², and even bending in Si–O–Si or Si–O–Al^{20,21}. Therefore, considering the qualitative analysis of infrared spectra of the oxide films produced by PEO in phosphate/silicate electrolytes, it can be concluded that the oxide films are composed by silica, alumina, mullite and hydroxides, as reported by other authors.

Considering the increase of the phosphate in the electrolyte, there was no significant change of the FTIR spectra of the PEO films. Some alteration is perceived below 550 cm⁻¹, probably related to crystalline phase modification of alumina. It is expected that this structure change leads to a modified morphology of the films so that they acquire better response to corrosion.

XRD analysis

Figure 3 shows the diffractograms of uncoated and PA aluminum alloy samples. As can be observed, Al alloy spectrum shows peaks of Al diffraction located at 38.5°, 44.8°, 65.1°, 78.2° and 82.5°, respectively correspondents to crystallographic planes of [111], [200], [220], [311] and [222], as reported by others researchers^{22,23}. Moreover, a short and crescent band in the range of 15°–30° is assumed to belong to the amorphous structure^{24–26} of the native alumina, as also noticed in the infrared analysis. The spectra of PA-treated samples show the same Al diffraction cited above plus different diffraction peaks at 37.7°, 39.5°, 45.9° and 67.1° recognized as γ -Al₂O₃, corresponding respectively to crystallographic planes of [311], [222], [400] and [440]²³.

The presence of Al diffraction in XRD analysis of PA layers can be justified by low thickness and porosity of oxide films. When the pores were not sealed during the discharges, Al diffraction cross them from substrate to surface, being detected by XRD equipment^{3,27}. By the way, some authors suggest that Al diffraction can be reduced as the density of the inner layer increases, which occurs with the sealing of the pores^{3,9,13}.

By observing the spectra, it is possible to note a decrease of Al diffraction intensities according to Na₃PO₄ proportion, which may be interpreted as a sodium phosphate ability for sealing of the pores created in the film structure. Besides, Na₃PO₄ addition seems to favor the elevation of the amorphous phases observed below 30°, including the mullite (3Al₂O₃·2SiO₂ or Al₆O₁₃Si₂)²⁶, which can also be identified at 15.8° and 60.9° diffraction peaks²⁴. The mullite is a needle-shaped crystal formed by chemical reaction between γ -Al₂O₃ and SiO₂, and it usually occurs when the electrolyte is composed of large amounts of silicon^{22,26,28}.

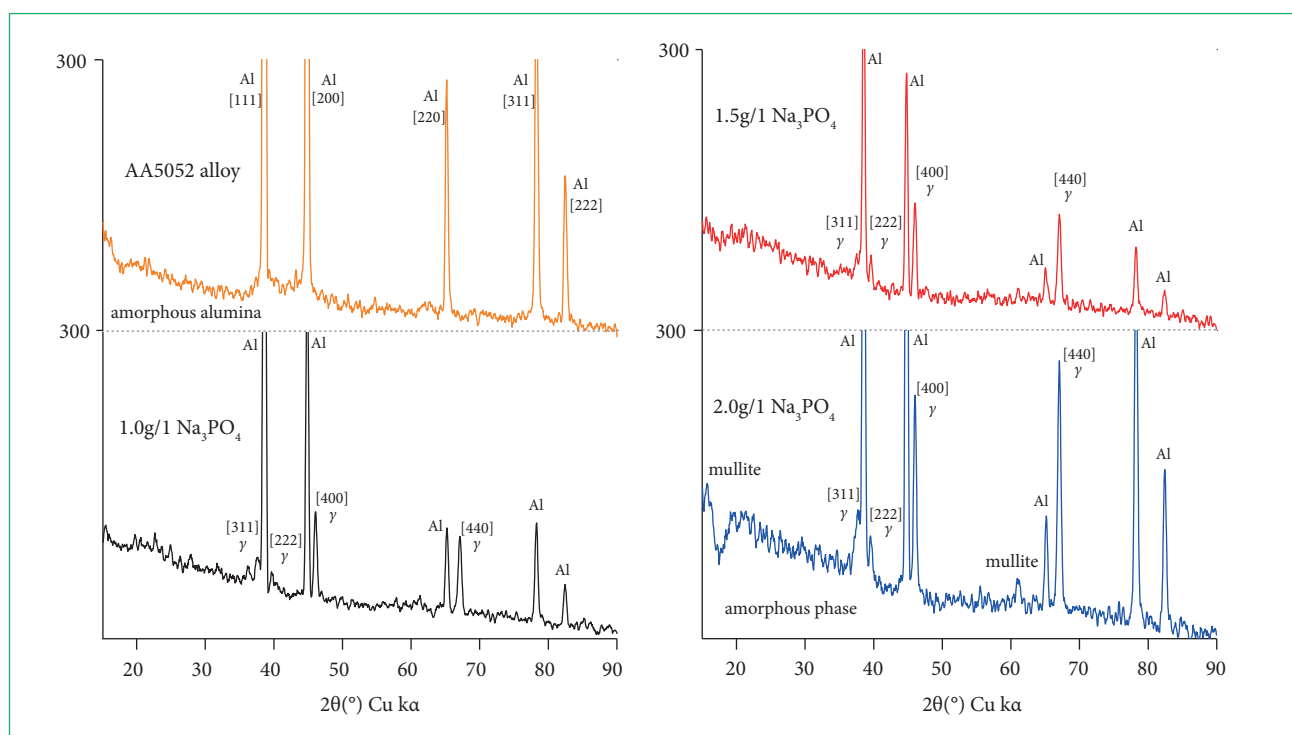


Figure 3: XRD diffractograms of 5052 Al alloy untreated and treated by plasma anodization.

The reduction of Al diffraction was confirmed by the highest peaks located at 38.5° and 44.8° , respectively shown in Fig. 4 (a) and (b); similar behavior occurred with remaining Al diffraction. Because of the lower Al diffraction peaks, it is expected that plasma anodization performed with 1.5 g/l Na_3PO_4 had produced alumina layer with the best densification of the inner layers. Notwithstanding, this can indicate a critical amount of Na_3PO_4 to create an oxide coating with an inner dense layer, because Al diffraction increased at process performed in higher amount of phosphate. Remarking the highest diffraction peaks of $\gamma\text{-Al}_2\text{O}_3$ centered at 45.9° and 67.1° , shown in Fig. 4 (c) and (d), it is perceived that Na_3PO_4 content favored the growth of the oxide layer. Although the formation mechanism of the layers is not clear, it seems that sodium phosphate contributed to its growth rate¹¹, whose structure is predominantly composed by $\gamma\text{-Al}_2\text{O}_3$ with higher diffraction intensity at 2.0 g/l Na_3PO_4 process.

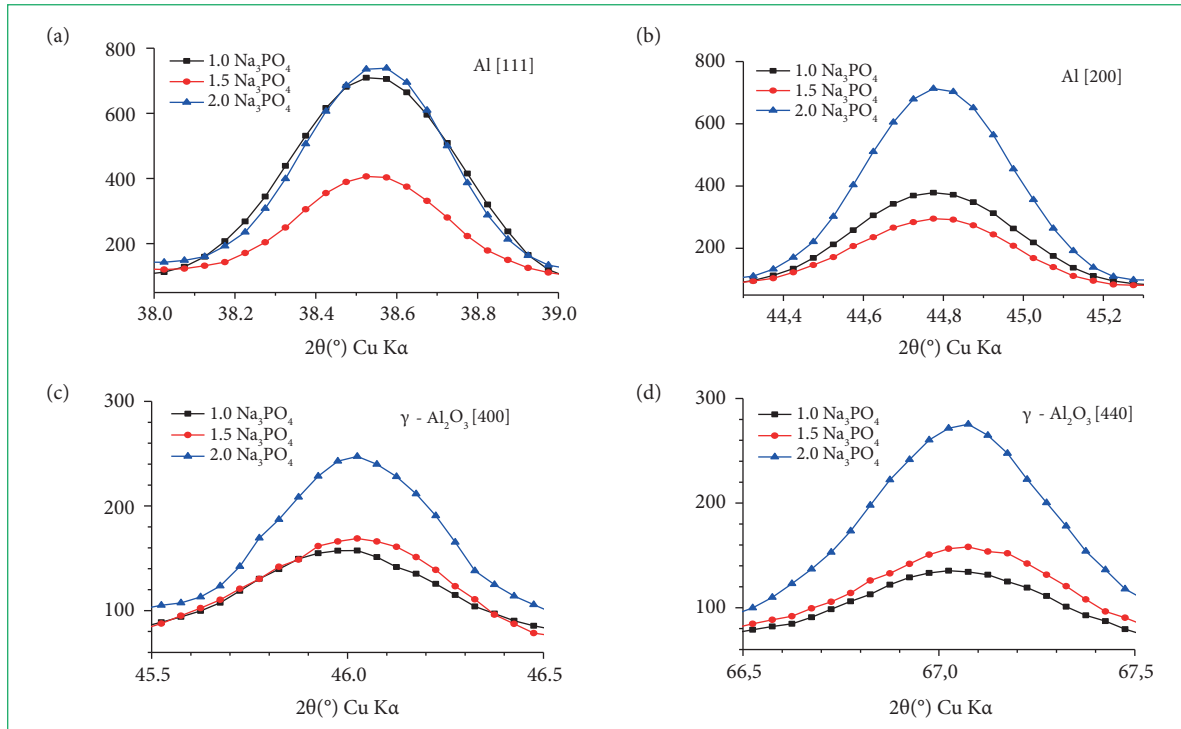


Figure 4: Diffractions peaks of Al [111] (a), Al [200] (b), $\gamma\text{-Al}_2\text{O}_3$ [400] (c) e $\gamma\text{-Al}_2\text{O}_3$ [440] (d), as function of Na_3PO_4 proportion.

Morphological analysis

Figure 5 presents the thickness (a) and the roughness (b) of the coatings, obtained statistically from 10 measures. The thickness of the films increased almost linearly as the phosphate content was gradually incremented, while the roughness was not significantly altered. Roughness presented measures around $1.1 \mu\text{m}$, and the thickness varied from 1.4 to $3.0 \mu\text{m}$. It is presumed that thickness measurements present some uncertainty due to nonuniformity of the oxide layers and their porous structures, which affect the Eddy-current gauge.

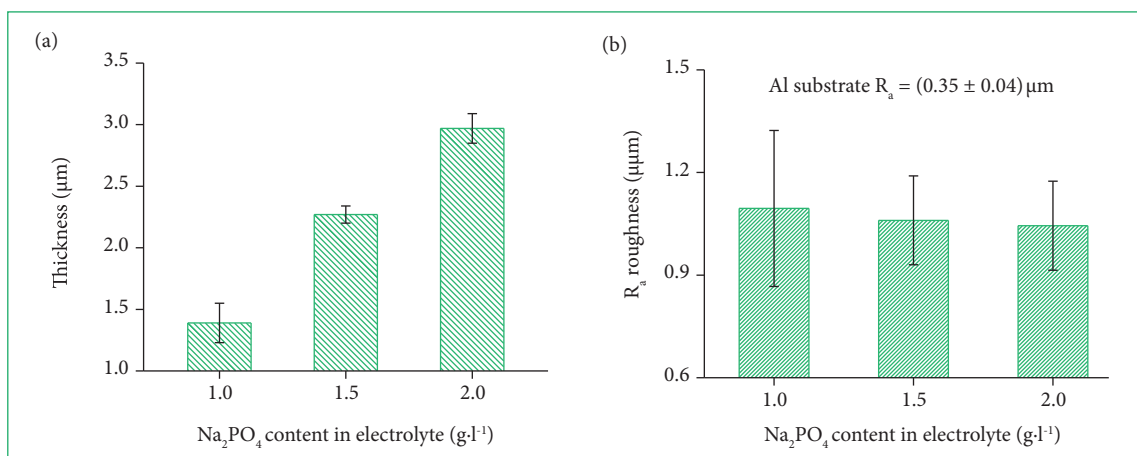


Figure 5: Thickness (a) and roughness (b) of the coatings deposited by plasma anodization for 10 min.

Figure 6 shows the micrography of the film surfaces obtained from plasma-anodized 5052 Al alloy, magnified in $950\times$. As can be observed, those films present a coralline morphology, which is a typical character of PEO coatings on aluminum substrates^{3,4}. The surface shows the presence of microcraters, spheroidal protuberances and filamentous structures, all of them at different sizes. Those filaments are monocystals of mullite, as cited in XRD analysis, and it seems to have been covered during the growth of the layer, as Na_3PO_4 was increased in the electrolyte. The increment of Na_3PO_4 content also looks to affect the size and distribution of those structures, but it did not modify statically the surface roughness, as shown above.

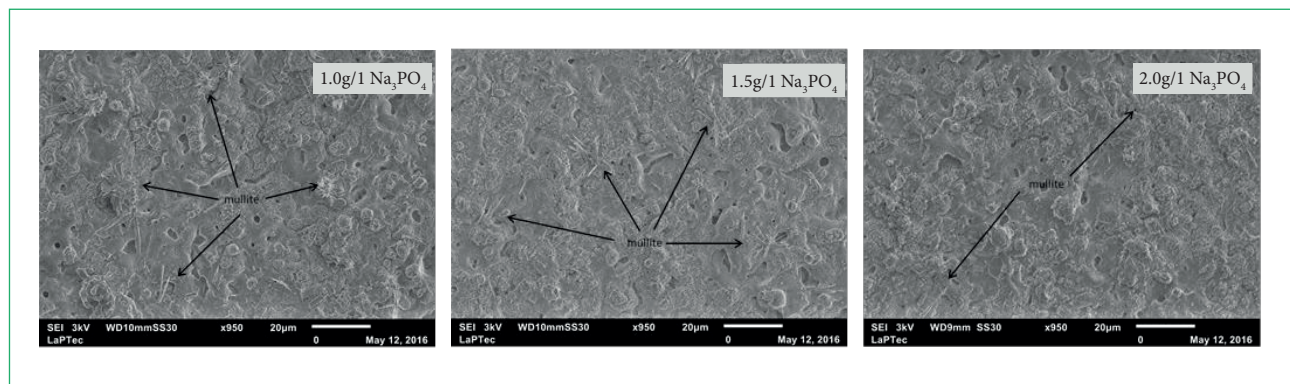


Figure 6: SEM images of oxide films deposited from a silicate electrolyte containing different amounts of phosphate (Na_3PO_4).

The elemental composition of the samples, presented in Table 1, was evaluated by EDX analysis using the images of $20\ \mu\text{m}$ -resolution and $10\ \text{kV}$ -energy. As can be seen, the substrate is composed by aluminum (Al), oxygen (O), carbon (C) and magnesium (Mg); Al and Mg are part of the 5052 Al alloy chemical composition, O belongs to atmosphere air and is responsible for Al oxidation and formation of native alumina (Al_2O_3). Carbon probably is a residual contaminant from diamond past used in the polishing or from atmospheric CO_2 , which can be adsorbed on the alumina surface due to chemical affinity¹⁵.

Figure 7 presents the oxide coatings are composed by elements from the Al alloy (Al, Mg) and species from the electrolyte (O, Si, Na), as ascribed in literature^{3,4}. Carbon atoms were also detected from coating surfaces, but their content is lower than that aluminum substrate. It is explained by the initial stage of anodizing which leads to dissolution of native alumina and the removal of other contaminants from the surface. Oxygen appears in atomic rate higher than 60%, but this proportion is slightly reduced with the increment of Na_3PO_4 in the electrolytic solution. Oxygen is the majority species of the structure followed by Si, Al and Na.

The increase of Na_3PO_4 content in the electrolyte caused a slight decrease in Si atomic rate, as occurred with O, and induced a slight fluctuation in Al and Na proportions, but kept both in smaller amounts than Si. Magnesium atoms just appear at the anodization performed in the electrolyte containing $1.5\ \text{g/l}\ \text{Na}_3\text{PO}_4$, in which the Na content was the lowest. Sodium atoms probably are related to NaOH species formed in solution and were introduced on the surface during the process^{29,30}. Meanwhile, it is possible that Na was ejected from the surface when Mg was moved from the substrate to electrolyte through the discharge channels. Although the phosphorus (P) is part of electrolyte, it was not detected in the oxide films, probably due to higher energy for chemical reaction compared to other species present in solution. Therefore, this analysis confirms that the oxide coatings grown via plasma anodization from silicate electrolytic

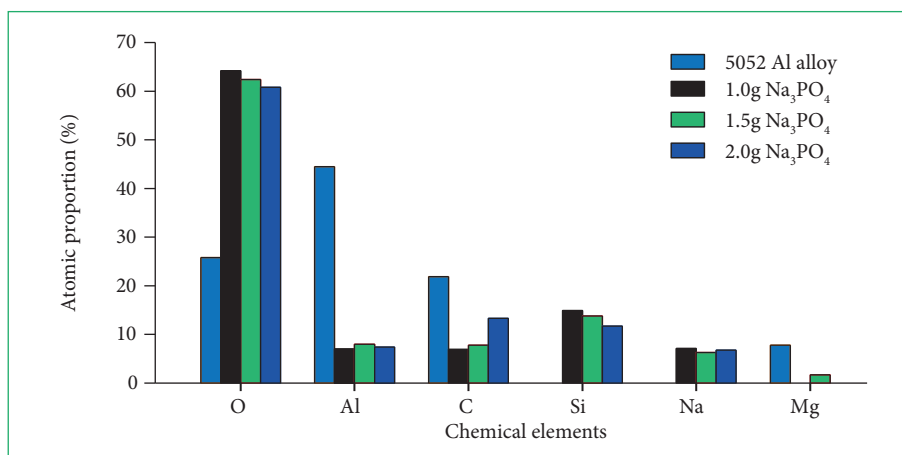


Figure 7: EDX analysis of oxide film surfaces deposited by plasma anodization from Na_2SiO_3 electrolyte containing small amounts of Na_3PO_4 .

solution with phosphate as additive are composed mainly of silica (Si_xO_y), and the coating structure is formed by a combination of silica and alumina (Al_2O_3), probably with Al and Na hydroxides adsorbed on the surface^{29,30}.

Corrosion behavior

The corrosion response of PA-treated and untreated 5052 Al alloy exposed to NaCl solution (3.5wt%) are shown in Fig. 8.

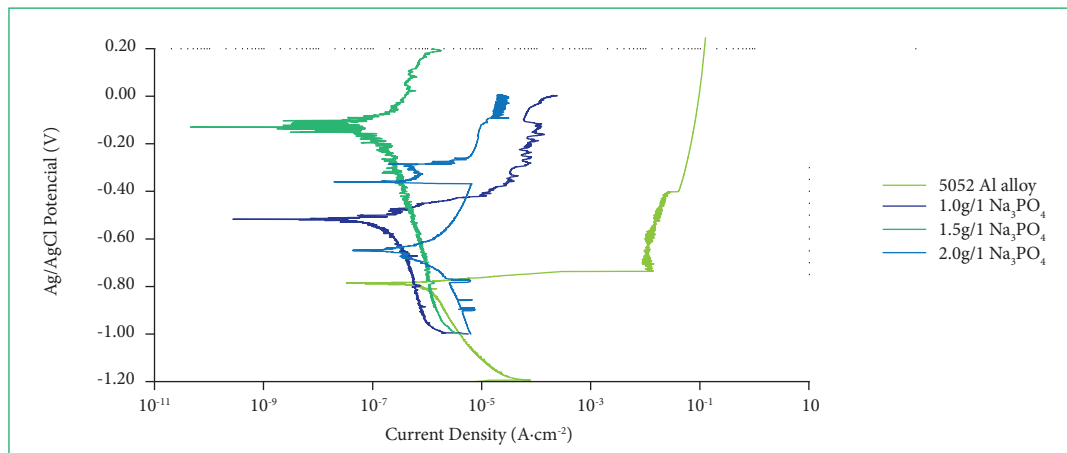


Figure 8: Corrosion behavior of untreated 5052 Al alloy and plasma-anodized samples in silicate-phosphate containing solution.

As can be seen, all the treated samples present a noble behavior compared to the untreated sample, as verified in others PEO researches^{31,32}. The corrosion potential increased from -0.79 to -0.12 V as the Na_3PO_4 content was raised. The higher corrosion potential was obtained at the treatment performed with 1.5 g/l Na_3PO_4 . This process presented higher Al content in its structure, as verified in elemental analysis, and, therefore, it is believed that the sample presents superior performance due to its higher content of alumina (Al_2O_3) than silicate (Si_xO_y). Besides, its structure can be denser than other coatings, as proposed in XRD discussion.

Table 1: Corrosion potential (E_{corr}) and corrosion current density (J_{corr}) of untreated Al alloy and plasma-anodized samples.

	5052 Al alloy	1.0 g/l Na_3PO_4	1.5 g/l Na_3PO_4	2.0 g/l Na_3PO_4
E_{corr} (V)	-0.79	-0.52	-0.12	-0.65
J_{corr} (Acm ⁻²)	3.5×10^{-7}	2.5×10^{-8}	2.2×10^{-8}	1.2×10^{-7}

The results obtained from linear extrapolation of Tafel curves are summarized in Table 1. Observing the current density of the samples exposed to NaCl solution (3.5 wt%), it was verified that samples anodized in lower content of phosphate presented a resistance to ion flux higher than one order of magnitude compared to the remaining ones. However, the treatment accomplished in the process with 1.5 Na_3PO_4 shows a value slightly higher than in 1.0 Na_3PO_4 . Differently, this last treatment led to two repassivations, and the stabilization of the current density occurred at four orders of magnitude lower than the bare 5052 Al alloy. This stabilization at a lower order of magnitude also occurred for the remaining anodizations, which also confirms the better performance of the PA-treated samples against the corrosion.

According to this electrochemical analysis, Al alloy samples achieved an improved corrosion resistance after the plasma anodization, and the chemical composition of the electrolytic solution seems to be important for such characteristic of the coatings on aluminum.

CONCLUSION

Oxide coatings were deposited at 10 min-plasma anodization on 5052 aluminum alloy using electrolyte composed by Na_2SiO_3 and Na_3PO_4 as additive. This additive contributed to the growth of the films, but did not cause significant changes in their surface roughness.

The FTIR analysis of the anodized coatings showed the presence of Al–O and Si–O vibration bands, respectively related to alumina and silica, and probably combination between those species. Some species were confirmed as crystalline phases detected by XRD equipment. This analysis shows that the anodized coatings are mainly composed by $\gamma\text{-Al}_2\text{O}_3$. Mullite ($\text{Al}_6\text{O}_{13}\text{Si}_2$) and amorphous species were also detected with the increment of Na_3PO_4 in the electrolyte.

The SEM analysis revealed surfaces slightly smooth and sealed pores as the phosphate was raised. It is presumed that the morphology of the coatings improved by the additive, and this structure is the responsible by corrosive response of the plasma anodized samples. Compared to bare 5052 Al alloy, all anodized samples shown a better resistance to corrosion.

However, the results show a limit to proportion of additive in which it no longer contributes to the coatings formation with crystalline phases and denser structure. Higher proportion of Na_3PO_4 promotes the transformation of crystalline phases in mullite and amorphous phases, which affect the morphology and corrosion behavior of the PA films.

FINANCIAMENTO

Fundação de Amparo à Pesquisa do Estado de São Paulo [<https://doi.org/10.13039/501100001807>]

#2014/19768-9

ACKNOWLEDGMENTS

Authors would like to thank National Space Research Institute (INPE-SP) and UNESP-Sorocaba for analysis instruments.

REFERENCES

- Sukiman NL, Zhou X, Birbilis N, Hughes AE, Mol JMC, Garcia SJ, et al. Durability and corrosion of aluminium and its alloys: overview, property space, techniques and developments. In: Ahmad Z. (Ed.). *Aluminium Alloys: New Trends in Fabrication and Applications*. London: IntechOpen; 2012. <https://doi.org/10.5772/53752>
- Hussein RO, Northwood DO. Production of anti-corrosion coatings on light alloys (Al, Mg, Ti) by plasma-electrolytic oxidation (PEO). In: Aliofkhaezai M. (Ed.). *Developments in Corrosion Protection*. London: IntechOpen; 2014. <https://doi.org/10.5772/57171>
- Li Q, Liang J, Wang Q. Plasma electrolytic oxidation coatings on lightweight metals. In: Aliofkhaezai M. (Ed.). *Modern Surface Engineering Treatments*. London: IntechOpen; 2013. <https://doi.org/10.5772/55688>
- Lugovskoy A, Zinigrad M. Plasma electrolytic oxidation of valve metals. In: Mastai Y. (Ed.). *Materials Science: Advanced Topics*. London: IntechOpen; 2013. <https://doi.org/10.5772/54827>
- Apelfeld AV, Ashmarin AA, Borisov AM, Vinogradov AV, Savushkina SV, Shmytkova EA. Formation of zirconia tetragonal phase by plasma electrolytic oxidation of zirconium alloy in electrolyte comprising additives of yttria nanopowder. *Surf Coat Technol.* 2017;328:513-7. <https://doi.org/10.1016/j.surfcoat.2016.09.071>
- Gunduz KO, Oter ZC, Tarakci M, Gencer Y. Plasma electrolytic oxidation of binary Mg-Al and Mg-Zn alloys. *Surf Coat Technol.* 2017;323:72-81. <https://doi.org/10.1016/j.surfcoat.2016.08.040>
- Vakili-Azghandi M, Fattah-Alhosseini A, Keshavarz MK. Optimizing the electrolyte chemistry parameters of PEO coating on 6061 Al alloy by corrosion rate measurement: response surface methodology. *Measurement.* 2018;124:252-9. <https://doi.org/10.1016/j.measurement.2018.04.038>
- Famiyeh L, Huang X. Plasma electrolytic oxidation coatings on aluminum alloys: microstructures, properties, and applications. *Mod Concept Material Sci.* 2019;2(1):000526.
- Wang J-H, Du M-H, Han F-Z, Yang J. Effects of the ratio of anodic and cathodic currents on the characteristics of micro-arc oxidation ceramic coatings on Al alloys. *Appl Surf Sci.* 2014;292:658-64. <https://doi.org/10.1016/j.apsusc.2013.12.028>
- Darband GB, Aliofkhaezai M, Hamghalam P, Valizade N. Plasma electrolytic oxidation of magnesium and its alloys: mechanism, properties and applications. *J Magnes Alloy.* 2017;5(1):74-132. <https://doi.org/10.1016/j.jma.2017.02.004>
- Wang Y, Chen M, Zhao Y. Preparation and corrosion resistance of microarc oxidation-coated biomedical Mg-Zn-Ca alloy in the silicon-phosphorus-mixed electrolyte. *ACS Omega.* 2019;4(25):20937-47. <https://doi.org/10.1021/acsomega.9b01998>
- Stefani R, Maia AD, Teotonio EES, Monteiro MAF, Felinto MCFC, Brito HF. Photoluminescent behavior of $\text{SrB}_4\text{O}_7:\text{RE}^{2+}$ (RE=Sm and Eu) prepared by Pechini, combustion and ceramic methods. *J Solid State Chem.* 2006;179(4):1086-92. <https://doi.org/10.1016/j.jssc.2006.01.006>
- Liu Z, Wang J, Kang M, Yin N, Wang X, Tan Y, et al. Synthesis of glycerol carbonate by transesterification of glycerol and dimethyl carbonate over $\text{KF}/-\text{Al}_2\text{O}_3$ catalyst. *J Braz Chem Soc.* 2014;25(1):152-60. <https://doi.org/10.5935/0103-5053.20130281>
- Rocha LVM. Revestimentos obtidos por oxidação da liga AA3104-H19 por plasma eletrolítico (PEO) [Dissertation]. [Campinas]: Universidade Estadual de Campinas, Faculdade de Engenharia Mecânica; 2013.
- Salem REP, Chinelatto ASA, Chinelatto AL. Synthesis of alumina powders by a modified Pechini method with addition of seeds in different calcination atmospheres. *Cerâmica.* 2014;60(353):108-16. <https://doi.org/10.1590/S0366-69132014000100016>

16. Prado LASA, Sriyai M, Ghislandi M, Barros-Timmons A, Schulte K. Surface modification of alumina nanoparticles with silane coupling agents. *J Braz Chem Soc.* 2010;21(12):2238-45. <https://doi.org/10.1590/S0103-50532010001200010>
17. Sarraf S, Zalnezhad E, Bushroa AR, Hamoda AMS, Baradaran S, Nasiri-Tabrizi B, Rafieerad AR. Structural and mechanical characterization of Al/Al₂O₃ nanotube thin film on TiV alloy. *Appl Surf Sci.* 2014; 321:511-519. <https://doi.org/10.1016/j.apsusc.2014.10.040>
18. Rosário DCC. Estudo da influência dos íons Mg²⁺ e Zr⁴⁺ na transição de fase amorfo-gama da alumina [Dissertation]. [São Paulo]: Escola Politécnica da Universidade de São Paulo, Departamento de Engenharia Metalúrgica e de Materiais; 2012.
19. Vargas AS, Schneider EL, Schmitz G, De Aquim, PM. Argamassas geopoliméricas à base de cinzas volantes álcali-ativadas contendo areia de fundição. *Cerâmica.* 2015;61(359):317-22. <https://doi.org/10.1590/0366-69132015613591784>
20. Lima AEA, Sales HB, Lima LC, Santos JCO, Santos IMG, Souza AG, et al. Natural clay applied to the clarification of used automotive lubricating oil. *Cerâmica.* 2017;63(368):517-23. <https://doi.org/10.1590/0366-69132017633682123>
21. Machado MCP, Langbehn JT, Oliveira CM, Elyseu F, Cargnin M, De Noni Junior A, et al. Study of the behavior and characterization of bentonitic clays after lyophilization process. *Cerâmica.* 2018;64(370):207-13. <https://doi.org/10.1590/0366-69132018643702324>
22. Martin J, Nominé A, Ntomprougkidis V, Migot S, Bruyère S, Soldera F, et al. Formation of a metastable nanostructured mullite during plasma electrolytic oxidation of aluminium in "soft" regime condition. *Mater Des.* 2019;180:107977. <https://doi.org/10.1016/j.matdes.2019.107977>
23. Khan RHU, Yerokhin A, Li X, Dong H, Matthews A. Surface characterisation of DC plasma electrolytic oxidation treated 6082 aluminium alloy: Effect of current density and electrolyte concentration. *Surf Coat Technol.* 2010;205(6):1679-88. <https://doi.org/10.1016/j.surfcoat.2010.04.052>
24. Lugovskoy A, Zinigrad M, Kossenko A, Kazanski B. Production of ceramic layers on aluminum alloys by plasma electrolytic oxidation in alkaline silicate electrolytes. *Appl Surf Sci.* 2013;264:743-7. <https://doi.org/10.1016/j.apsusc.2012.10.114>
25. Dehnavi V, Liu XY, Luan BL, Shoesmith DW, Rohani S. Phase transformation in plasma electrolytic oxidation coatings on 6061 aluminum alloy. *Surf Coat Technol.* 2014;251:106-14. <https://doi.org/10.1016/j.surfcoat.2014.04.010>
26. Aliasghari S, Ghorbani M, Skeldon P, Karami H, Movahedi M. Effect of plasma electrolytic oxidation on joining of AA 5052 aluminium alloy to polypropylene using friction stir spot welding. *Surf Coat Technol.* 2017;313:274-81. <https://doi.org/10.1016/j.surfcoat.2017.01.084>
27. Treviño M, Garza-Montes-de-Oca NF, Pérez A, Hernández-Rodríguez MAL, Juárez A, Colás R. Wear of an aluminium alloy coated by plasma electrolytic oxidation. *Surf Coat Technol.* 2012;206(8-9):2213-9. <https://doi.org/10.1016/j.surfcoat.2011.09.068>
28. Oter ZC, Azakli Y, Cengiz S, Gencer Y, Tarakci M. Microarc oxidation of pure aluminium in alumina containing electrolytes. *Surf Eng.* 2019. <https://doi.org/10.1080/02670844.2019.1698162>
29. Snizhko LO, Yerokhin AL, Gurevina NL, Misnyankin DO, Pilkington A, Leyland A, Matthews A. A model for galvanostatic anodizing of Al in alkaline solutions. *Electrochim Acta.* 2005;50(27):5458-64. <https://doi.org/10.1016/j.electacta.2005.03.052>
30. Rudnev VS, Lukiyanchuk IV, Kuryavyi VG. Electrolytic-plasma oxidation in borate electrolytes. *Prot Met.* 2006;42(1):55-9. <https://doi.org/10.1134/S0033173206010103>
31. Dai L, Li W, Zhang G, Fu N, Duan Q. Anti-corrosion and wear properties of plasma electrolytic oxidation coating formed on high Si content Al alloy by sectionalized oxidation mode. *IOP Conf Ser: Mater Sci Eng.* 2017;167:012063. <https://doi.org/10.1088/1757-899X/167/1/012063>
32. Sieber M, Simchen F, Morgenstern R, Scharf I, Lampke T. Plasma electrolytic oxidation of high-strength aluminium alloys—substrate effect on wear and corrosion performance. *Metals.* 2018;8(5):356. <https://doi.org/10.3390/met8050356>